

ADHESION AND OSTEOGENIC DIFFERENTIATION OF HUMAN MESENCHYMAL STEM CELLS ON TITANIUM NANOPORES

Sandrine Lavenus^{1,2,*}, Martine Berreur¹, Valerie Trichet¹, Paul Pilet^{3,4}, Guy Louarn² and Pierre Layrolle¹

¹ LPRO, Inserm U957, Nantes, France

² CNRS - Institut des Materiaux, Nantes, France

³ LIOAD, Inserm U791, Nantes, France

⁴ CHU Nantes, Nantes, France

Abstract

Titanium implants are widely used in orthopaedic and dental surgery. Surface properties play a major role in cell and tissue interactions. The adhesion and differentiation of mesenchymal stem cells were studied as a function of nanostructures. Titanium surfaces with nanopores 30, 150 and 300 nm in diameter were prepared by physical vapour deposition. PCR arrays indicated that the expression of integrins was modulated by the nanopore size. Human Mesenchymal Stem Cells (hMSCs) exhibited more branched cell morphology on Ti30 than on other surfaces. Ti30 and Ti150 induced osteoblastic differentiation while Ti300 had a limited effect. Overall, nanopores of 30 nm may promote early osteoblastic differentiation and, consequently, rapid osseointegration of titanium implants.

Keywords: Titanium nanopores, mesenchymal stem cells, cell adhesion, cell morphology, integrins, osteogenic differentiation.

Introduction

Titanium implants are widely used in dental and orthopaedic surgery because of favourable mechanical and biocompatible properties. Numerous studies have shown that the early events of bone healing around implants are related to their long-term clinical success (Davies, 2003; Marco *et al.*, 2005). In order to promote the osseointegration of implants, various surface treatments have been proposed. The objective of these surface treatments is to improve protein adsorption, cell adhesion and differentiation and consequently, the tissue integration of titanium implants. It has been recently shown that nanometre-sized features control the adhesion and osteogenic differentiation of cells (Dalby *et al.*, 2007b; Le Guéhennec *et al.*, 2007) but these results have not been confirmed on titanium.

Most studies have examined the osteogenic potential of implant surfaces *in vitro* by using immature osteoblast or osteoblast cell lines (Dalby *et al.*, 2006a; Dalby *et al.*, 2006b; Le Guéhennec *et al.*, 2008a; Le Guéhennec *et al.*, 2008b). However, the first cells to colonise the surface after implantation, are mesenchymal stem cells (MSCs). Peripheral MSCs are attracted into the peri-implant region by chemo-attractant molecules and are able to migrate through the blood clot to colonise the implant surface (Caplan *et al.*, 2006; Caplan, 2009). MSCs are multipotent cells present in blood, bone marrow and other tissues at low levels. Under the control of specific cues (e.g., cytokines, growth factors, or micro-environment), MSCs have the capacity to differentiate into osteoblasts (Marinucci *et al.*, 2010), chondroblasts (Zannettino *et al.*, 2008), myoblasts (Engler *et al.*, 2006) and adipocytes (Morganstein *et al.*, 2010). The nature of the tissue around implants may well depend on the differentiation of MSCs induced by their surface properties (Engler *et al.*, 2006; Kassem, 2006; Protivínský *et al.*, 2007; Lavenus *et al.*, 2010).

The first event after implantation is the adsorption of blood proteins on the surface of the implant. The nature and conformation of proteins on the implant are regulated by surface properties, in particular chemical composition, wettability and micro- and nano- topography (Cai *et al.*, 2006; Protivínský *et al.*, 2007). It has been shown that nanotopography does not only control protein adsorption, but also cell morphology and adhesion (Yang *et al.*, 2002; Zhao *et al.*, 2007). *In vitro* experiments have shown that cells can respond to their micro-environment (Curtis and Varde, 1964; Engler *et al.*, 2006). Other studies have demonstrated that nanotopography influenced cell behaviour (Curtis *et al.*, 2001; Stevens and George, 2005; Dalby *et al.*, 2007a; Dalby *et al.*, 2007b). Surface topography induced mechanical stress in the cytoskeleton

*Address for correspondence:

Sandrine Lavenus
LPRO, Inserm U957
1, rue Gaston Veil
F-44035 Nantes, France

Telephone Number : +33 (0)2 72 64 11 43

FAX Number : +33 (0)2 40 41 28 60

E-mail: sandrine.lavenus@univ-nantes.fr

that controls gene expression and thus differentiation (Watson, 1991; Kilian *et al.*, 2010; Olivares-Navarrete *et al.*, 2010).

While the nature of cell adhesion and the degree of cytoskeletal tension are widely accepted as affecting stem cell behaviour, the precise role of nanotopography on the adhesion, morphology and differentiation of cells has not yet been established. However, the use of nanoscale disorders to stimulate human MSC (hMSC) differentiation and promote bone mineralisation *in vitro* has been demonstrated in the absence of osteogenic factors (Engler *et al.*, 2006). However, these results have not been reproduced on the titanium substrates that are of high relevance for orthopaedic and dental applications. In view of this, Olivares-Navarrete *et al.* (2008) studied integrin $\alpha 2\beta 1$ expression and osteogenic differentiation of osteoblastic cells on Ti microstructures. Here, we have used physical vapour deposition (PVD) to coat nanoporous polycarbonate membranes to produce titanium substrates with controlled size nanostructure (30, 150 and 300 nm in diameter), but random distribution. We set out to examine whether changes in pore diameters could modify the cell shape, number of focal point or expression of integrin on human MSCs cultured on these substrates from hours to days. Using an image analysis and PCR array, we show the influence of pore diameter on hMSC adhesion. Previous studies have shown that changes in cell shape or integrin expression could regulate commitment of mesenchymal cells to different lineage (Olivares-Navarrete *et al.*, 2008; Lavenus *et al.*, 2011). Hence, the osteogenic differentiation of hMSCs on the nanostructured Ti was compared with Ti planar substrates with or without osteogenic supplements.

Materials and Methods

Materials

Polycarbonate membranes with nanometre sized pores measuring 30, 150 and 300 nm in diameter were purchased from Whatman (Nucleopore™, Invitrogen/Life Technologies, Villebon sur Yvette, France). The membranes were punched into discs measuring 14 mm in diameter. Glass coverslip discs, 14 mm in diameter, were also used (VWR, Fontenay sous Bois, France). The materials were coated with a thin layer of titanium by physical vapour deposition (PVD). About 30 samples were placed in a chamber at 10^{-6} mbar using a vacuum evaporation apparatus equipped with a turbomolecular pump (Alcatel 550 Turbo, Annecy, France). The sublimation of titanium was conducted at 100 A in a molybdenum crucible using a current generator (Eurotherm 94, Worthing, UK) in order to reach its sublimation temperature under vacuum (~1450 °C). The thickness of the titanium film was monitored using a quartz balance installed inside the evaporation chamber. A 5 nm thick titanium film was uniformly deposited on glass and membrane discs in 30-90 s. After coating, the samples were cleaned in 70 % ethanol, then in deionised water and finally air-dried. The materials were sterilised with ethylene oxide after double packaging in sealed bags. The glass coverslip discs coated with a thin titanium layer were abbreviated Ti and used as controls. The membranes

with nanopores coated with titanium were named Ti30, Ti150 and Ti300.

Physical and chemical analysis of the surfaces

Three samples from each group ($n = 3$) were analysed by scanning electron microscopy (SEM, LEO VP1450, Zeiss, Oberkochen, Germany), atomic force microscopy (AFM) and X-ray photoelectron spectroscopy (XPS, Leybold LHS12; OC Oerlikon, Pfäffikon, Switzerland). XPS analysis of the surfaces was conducted using an aluminium K_{α} X-ray radiation source at 1486.6 eV and Scan system control. The pressure in the chamber was less than 2.7×10^{-7} Pa before the data were taken, and the voltage of the anode was 12 kV.

Cell culture

Human MSCs were obtained from bone marrow cell aspirations harvested in the iliac crest of patients undergoing orthopaedic surgery and after receiving informed consent (Etablissement Français du Sang, Centre-Atlantique, Tours, France). The experiments were repeated with at least 3 different bone marrow cell aspirations from patients of different age, sex and origin. Bone marrow cells were plated in 75 cm² tissue culture flasks (Corning, Corning, NY, USA) with 15 mL of culture medium. Standard culture medium consisted of alpha modified Eagle medium (α -MEM, Gibco, Invitrogen, Carlsbad, CA, USA) supplemented with 10 % foetal calf serum (FCS, Biotech GmbH, Aidenbach, Germany), 2 mM of L-glutamine, 100 μ g/mL of streptomycin and 100 units/mL of penicillin. The culture medium was refreshed every 2 d and adherent hMSC were cultured until 80 % confluence in a humidified atmosphere, 5 % CO₂ at 37 °C. Cells were detached using trypsin/EDTA (0.05 % v/v, Gibco, Invitrogen) for 5 min. In order to test the different substrates with a homogenous cell population, the hMSC were cryopreserved at the end of the first passage. Prior to seeding on the different substrates, the cells were thawed and cultured in 75 cm² flasks for 2-4 d. At confluence, the cells were harvested using trypsin-EDTA and counted on Malassez's hemocytometer using trypan blue exclusion dye.

Cell seeding on the surfaces

Ti30, Ti150 and Ti300 membrane discs were put into 12-well dishes and blocked using a glass cylinder with an internal diameter of 14 mm. All substrates including the Ti control had a surface of 2 cm². Three samples per group were used and the experiments were reproduced at least three times. Cell suspensions (500 μ L) were rapidly (less than 10 min) poured into each well at a density of 10,000 cells/cm². Cells were cultured on to the different substrates for 2 and 4h, and 1, 6, 12, 18 and 21 d.

Actin, vinculin and nuclei staining

hMSC were seeded and incubated on the different substrates for 2 and 4 h, and 1 and 6 d as described above. After removing the culture medium, the wells were rinsed three times with phosphate buffer saline (PBS, Gibco, Invitrogen). The cells were fixed with 4 % paraformaldehyde (Sigma, St. Quentin Fallavier, France) for 20 min and then washed three more times to remove

Table 1. Gene names and sequence primers for qPCR.

Human genes				PCR product length
Name	NM number	Forward primer	Reverse primer	
RPL19	000981	gctcttctcttcgctgct	cattggctcattgggtct	122 nt
ITG α 3	002204	tccgagtcactgtccacaga	gctgggctaccctattctc	88 nt
ITG α 4	000885	ccttgtttagtcaattactcttggga	ccggccatccatttaga	104 nt
ITG α V	002210	ccttgctgctcttggaaactc	attctgtggctgtcggagat	74 nt
ITG β 1	002211	acaccagcagccgtgtaac	ttcgatgccatcatgcaa	73 nt
ITG β 5	002213	gaggatgctaccgaccacag	gtccaacctgaccgtcctc	88 nt
LAMA2	000426	aattgaagaagccggatttg	tgttttggccctgtatctg	76 nt
RUNX2	004348	ggcccacaaatctcagatcgtt	cactggcgtgcaacaagac	184 nt
COL1a1	000088	acatggaccagcagactggca	tcactgtcttggcccaggct	153 nt
BSP	004967	cgaatacacggcgctcaatg	gtagctgtactcatctcatagggc	109 nt
OCN	199173	ggcgctacgtgtatcaatgg	tcagccaactgctcacagtc	106 nt
ALP	000478	aacaccaccagggggaac	ggtcacaatgccacagatt	78nt

excess paraformaldehyde. Samples were stored at 4 °C until staining for actin, vinculin and nuclei. Fixed cells were first permeabilised with PBS-0.5 % Triton (x100, Sigma) at 4 °C for 15 min. In order to reduce non-specific background, samples were blocked with PBS containing 1 % bovine serum albumin (BSA, Sigma) for 10 min at 37 °C. After blocking, the PBS/BSA was discarded and the samples were first incubated for 1 h with Alexafluor 488-phalloidin (Molecular Probe, Invitrogen, Cergy Pontoise, France) at a dilution of 1:40 in 10 mg/mL BSA in PBS at 37 °C in the dark. Between each incubation, the samples were rinsed twice with PBS-0.05 % Tween (Sigma). Antivinculin (Monoclonal anti-vinculin clone hVIN-1, Sigma) at a dilution of 1:100 in 1 % BSA/PBS was added to each well for 1 h at 37 °C in the dark and 30 min with secondary rabbit anti-mouse antibody (A11061, Molecular Probe, Invitrogen) at a dilution of 1:200 at room temperature. Finally, samples were incubated with Hoechst (Sigma) for 10 min at room temperature, and washed twice with deionised water. Samples were stored at 4 °C before fluorescence imaging (Nikon Eclipse, TE2000E, Champigny Sur Marne, France).

Image analysis of cell morphology

After staining the actin, vinculin and nuclei, fluorescent images were analysed with a custom-made program using an image analysis system (Quantimet Q550, Leica, Wetzlar, Germany). Four images were recorded at a magnification of x10 and x20 for each staining. A semi-automatic binary treatment was performed on each image. The number of cells attached to the substrates was automatically counted using nuclei staining. Actin staining was used for identification of cell shape into round, branched and spindle cell morphology. Cell areas were also measured for each type of cell morphology, giving insights into surface cell spreading. The number of focal points was counted per cell for each type of cell morphology and normalised by the

cell areas for each cell morphology. For each condition, a range of 80 to 300 cells was analysed.

PCR array and Real-time RT-qPCR assay

RT profiler PCR arrays for Human Extracellular Matrix and Adhesion Molecules (PAHS-013D, SA Biosciences, Tebu-bio, Le Perray en Yvelines, France) were first used to reveal genes, the expression of which may change depending on the nanostructured surface. For PCR arrays, hMSCs were seeded on substrates at a density of 10,000 cells/cm², as previously described. In order to obtain sufficient RNA concentration, 12 and 4 replicate wells were pooled for days 1 and 6, respectively. The cells were lysed and total RNA was extracted using a Macherey-Nagel Nucleospin RNA XS kit. Total RNA was quantified by spectrophotometer at the 260 nm wavelength (Nanodrop, Labtech, Palaiseau) and RNA quality was assessed using an Agilent Bioanalyser 2100 (Agilent Technologies, Santa Clara, CA, USA). After quantification and quality control, the PCR array was performed according to manufacturer's instructions. Online software from Tebu-bio was used to detect expressed genes (<http://www.sabiosciences.com>). Genes selected by PCR array analysis were validated by using real-time reverse-transcriptase polymerase chain reaction (RT-qPCR). The same culture conditions as previously described were used and experiments were reproduced at least 3 times. Total RNA (250 ng) was used for cDNA synthesis at 37 °C for 1 h with 0.5 μ g random primers (Promega, Charbonnière, France) 5X RT buffer, 0.5 mM dNTP mix (Eurobio, Les Ulis, France), 20U RNaseOUT and 400U M-MLV reverse transcriptase. The real-time PCR contained 5 ng cDNA, 300 nM forward and reverse primers and 5 μ L 2x SYBR green buffer (Bio-Rad, Marnes la Coquette, France) in a final volume of 10 μ L. Polymerase chain reactions were carried out in triplicate from several RNA extractions, in 96-well plates using the Chromo4 System (Bio-Rad). The oligonucleotides used were synthesised by Eurogentec (Angers, France) for

ITG α 3, ITG α 3, ITG α 3, ITG β 1, ITG β 5 and LAMA2 as described in Table 1.

Differentiation gene expression

hMSCs were seeded on Ti and cultured with standard or osteogenic medium (Ti osteo). Cultures on Ti nano with standard medium were also performed. The osteogenic medium consisted of standard medium supplemented with 10 mM of β -glycerophosphate (Sigma), 0.2 mM ascorbic acid (Sigma) and 10^{-8} M dexamethasone (Sigma). Total RNA was extracted using a Macherey-Nagel Nucleospin RNA XS kit after 6, 12 and 21 d of culture in control and osteogenic medium on the different surfaces. After quantification and quality control, RT-qPCR was performed as previously described. The oligonucleotides used were synthesised for RUNX2, COL1A1, BSP, OCN and ALP, as described in Table 1.

Alizarin red staining

Alizarin red staining was performed after 28 d of culture in order to corroborate osteogenic gene expression. The mineralisation assay was determined on each substrate in both standard and osteogenic media. The culture medium was discarded, confluent cell layers were washed with PBS and staining with Alizarin Red S (2 %, pH 4.2, Merck) was performed for 2 min. After aspiration of the overflow, cells were washed 3 times with water. Staining layers were visualised with binoculars and phase microscopy using an inverted microscope (Nikon).

Statistical analysis

Samples were characterised in triplicate in order to guarantee the consistency of the physical and chemical analysis ($n = 3$ /group). Cell culture experiments were reproduced at least three times using 3 samples per group. Data were averaged with the standard error of the mean (S.E.M). Statistical analysis was performed using ANOVA (SPSS 16.0 software; IBM SPSS, Armonk, NY, USA) and considered significant for $p < 0.05$.

Results

Surface characterisation

Fig. 1 shows the plain and nanoporous titanium coated surfaces. The control Ti group consisted of a thin layer of titanium uniformly deposited on the glass cover slips (Fig. 1a). SEM and AFM observations indicated that the average surface roughness (Ra) of Ti was 0.2 nm over $5 \times 5 \mu\text{m}^2$ (data not shown). The titanium coating was also uniform on the nanoporous polycarbonate membranes (Fig. 1b-d). The nanopores were not closed by the layer of titanium that was between 5.0 and 5.7 nm thick. Pore diameters and density are reported in Table 2. The pore diameters were 33.4, 148.9 and 293.1 nm for membranes Ti 30, Ti 150 and Ti 300, respectively. The chemical composition of the Ti coating was also determined by XPS (Fig. 1e). All coated substrates exhibited peaks corresponding to titanium oxide (TiO $_2$) as well as oxygen and carbon resulting from the polycarbonate membrane.

Cell morphology and focal point density

In order to identify the state of cell adhesion on the substrates, 3 different cell shapes were determined. As shown in Fig. 2, round, branched and spindle cell shapes were identified after 2 and 4 h, and 1 and 6 d on the different substrates. The initial state of adhesion was characterised by round morphology (Fig. 2a). Examples of branched and spindle cell morphology are shown in Fig. 2b and 2c, respectively. We have previously determined that hMSCs cultured for 24 h on tissue culture polystyrene (TCPS) had a prominent spindle fibroblastic shape while osteoblastic cells exhibited a branched shape (Le Guehennec *et al.*, 2008). The quantitative assessment of cell morphology on Ti (control) and Ti30, Ti150 and Ti300 is shown in Fig. 2d. Overall, the number of round cells decreased with culture time. After 1 and 6 d, the number of round cells remained around 5 %, probably as a result of cell division.

After 2 and 4 h, hMSCs had a prominent branched shape whatever the substrate. After 1 d, cells exhibited differences in cell morphology as a function of the surface. Cells had a predominantly typical spindle shape, with 58 and 61 % on Ti and Ti300, respectively. On the Ti30 surface, cells exhibited mainly a branched shape whereas the percentages of branched and spindle cells were comparable for Ti150. After day 6, the number of spindle shaped cells was higher on Ti150 (45 %) while the proportions were similar (20 %) for all other surfaces.

Fig. 3 shows the number of focal points as a function of cell morphology, culture time and surface. The number of focal points was first determined without identifying cell morphology (Fig. 3a). Focal point density increased with culture time indicating the cells spreading on substrates. After 2 h, a significantly greater focal point density was observed on Ti 300 whereas after 4 h, the density was higher on Ti 30 than on other surfaces. After 1 d, Ti150 exhibited a significantly higher number of focal points than on the Ti control group, but reached a plateau. After 6 d, the densities were higher for Ti30 and Ti300 than for other substrates. Following the significant effect of nanotopography for all shapes, focal point density was identified as a function of branched and spindle morphology. Round morphology was not considered as relatively low in proportion. Fig. 3b shows focal point density for the branched shape. A similar trend was observed for gathered shapes. The differences in focal point appeared prominent for the spindle morphology at day 6 (Fig. 3c). Focal point densities were greater for cells cultured on nanoporous titanium substrates compared to the planar Ti control. However, differences were not found between surfaces for other culture times. Generally, focal point density was greater on Ti30, and these surfaces seemed more suitable for cell adhesion.

Table 2. Diameter and pore density of pores on Ti 30, Ti 150 and Ti 300.

	Ti 30	Ti 150	Ti 300
Pore size (nm)	33.4 \pm 0.7	148.9 \pm 1.8	293.1 \pm 1.6
Density per μm^2	8.9 \pm 0.9	2.8 \pm 0.3	1.2 \pm 0.1

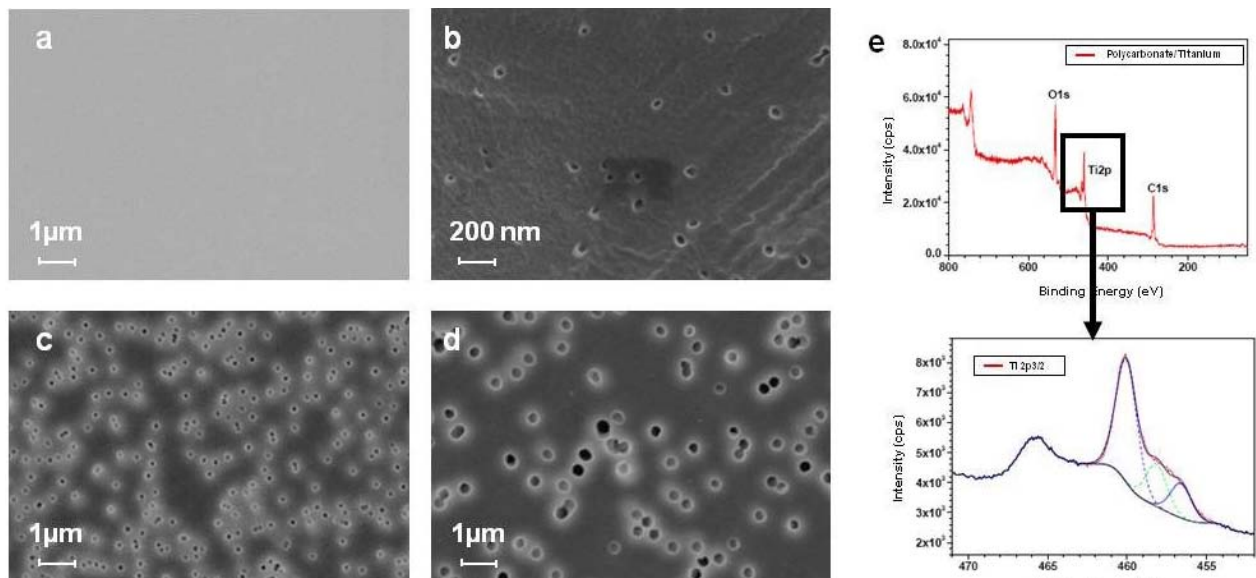


Fig. 1. Characterisation of plain and nanoporous titanium substrates by scanning electron microscopy and X-ray photoelectron spectroscopy. SEM micrographs of (a) Ti, (b) Ti30, (c) Ti150, (d) Ti300, and (e) representative XPS spectra of titanium-coated surfaces.

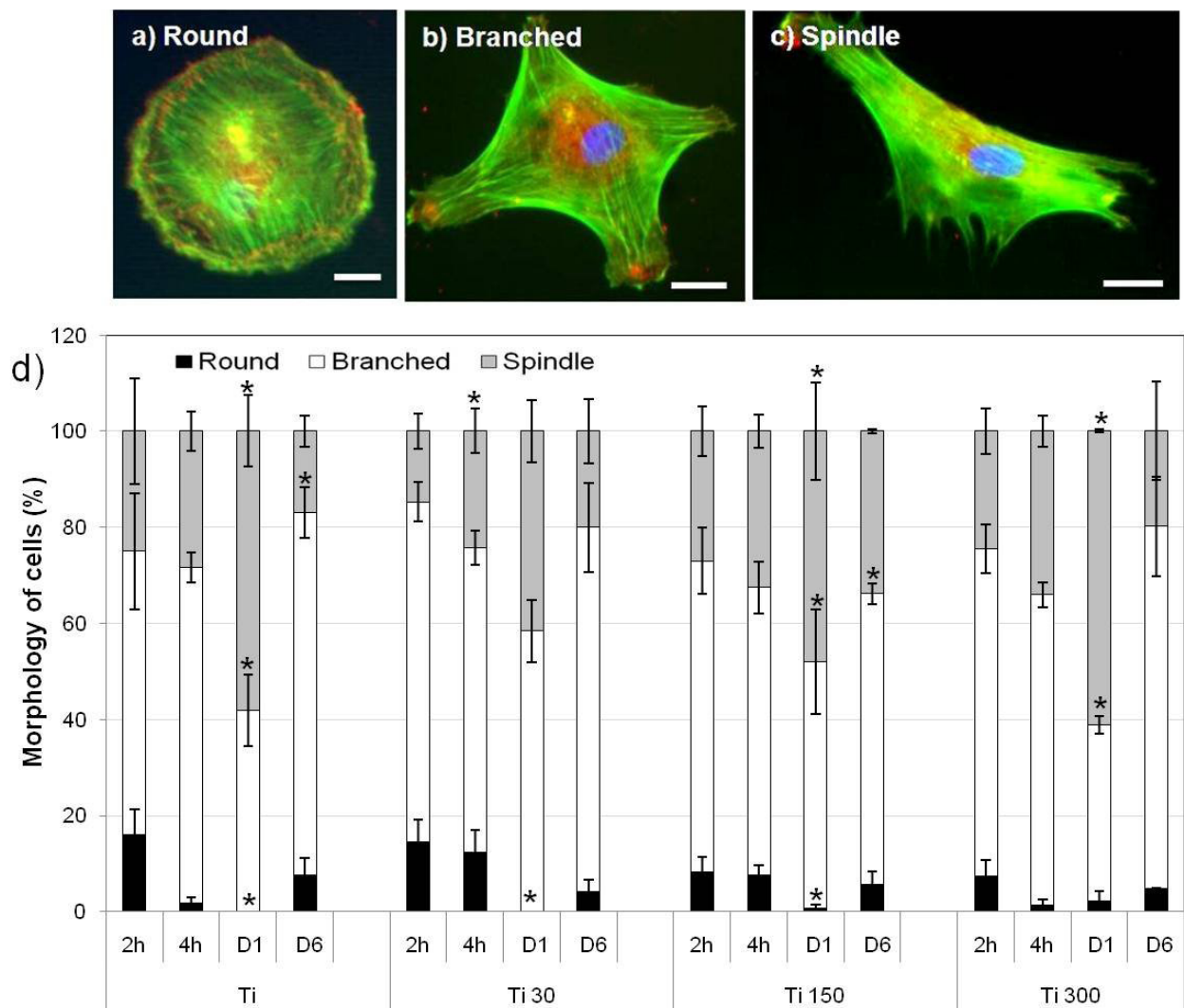


Fig. 2. Analysis of cell morphology on the nanoporous titanium substrates. Representative fluorescence images of hMSCs cultured on nanoporous Ti after staining of actin (green), vinculin (red) and nuclei (blue). (a) round, (b) branched and (c) spindle-shaped cell morphology, scale bars = 20 µm; (d) Quantitative image analysis of cell morphology as a function of substrates for hMSC cultured for 2, 4 h, 1 and 6 d of cultured on Ti, Ti30, Ti150 and Ti300. n = 30-100 cells counted per condition. (mean ± S.E.M.; * $p < 0.05$ as compared to Ti).

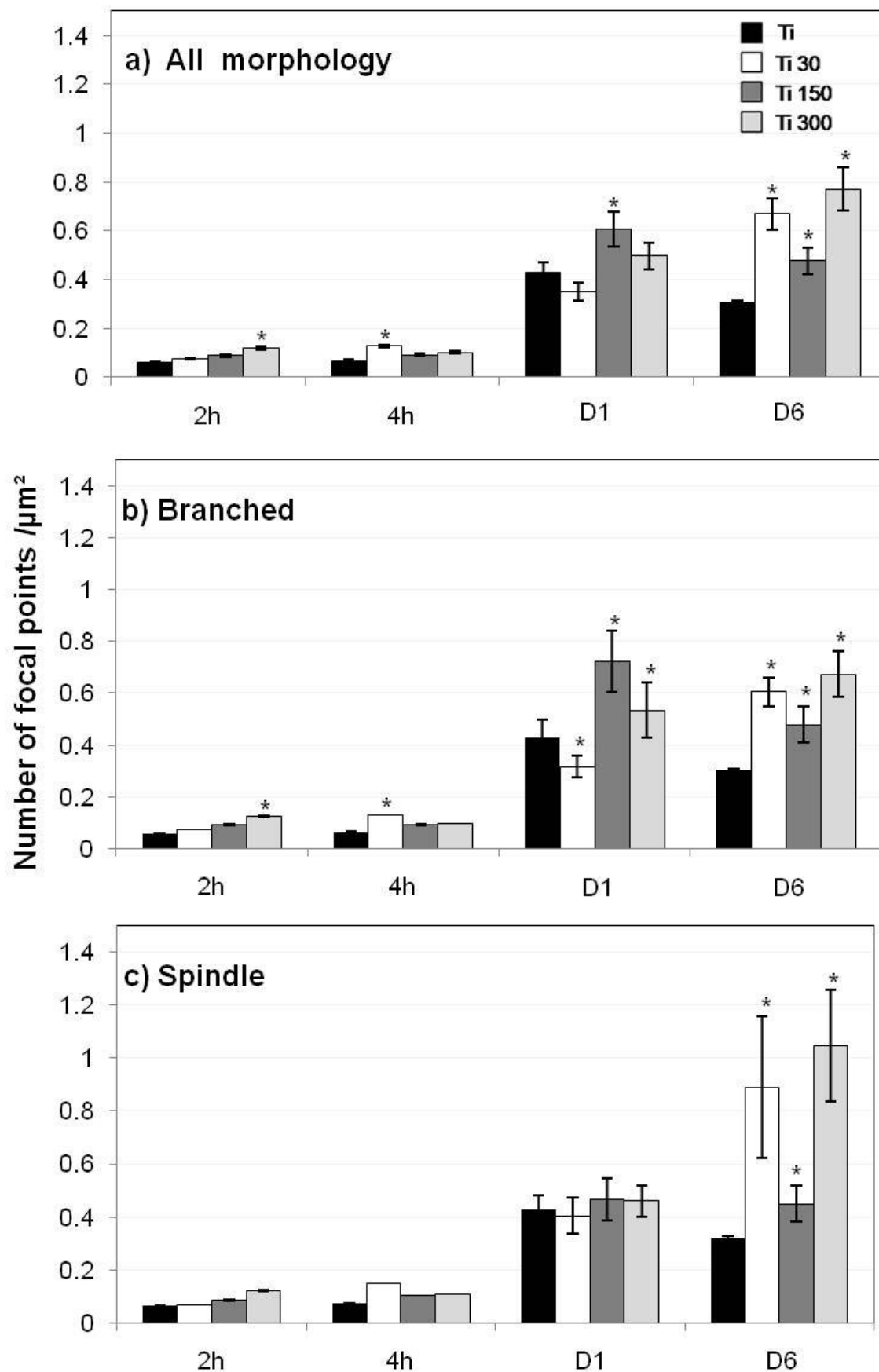


Fig. 3. Number of focal adhesion points per surface area as a function of culture time on the different substrates. Focal point density for a) all cell morphology b) branched and c) spindle morphology. The number of focal adhesion points was determined per μm^2 after 2 h, 4 h, 1 and 6 d after cell seeding on Ti, Ti30, Ti150 and Ti300 surfaces. $n = 30-100$ cells per condition. (mean \pm S.E.M) * $p < 0.05$, significant difference compared to Ti from the corresponding value.

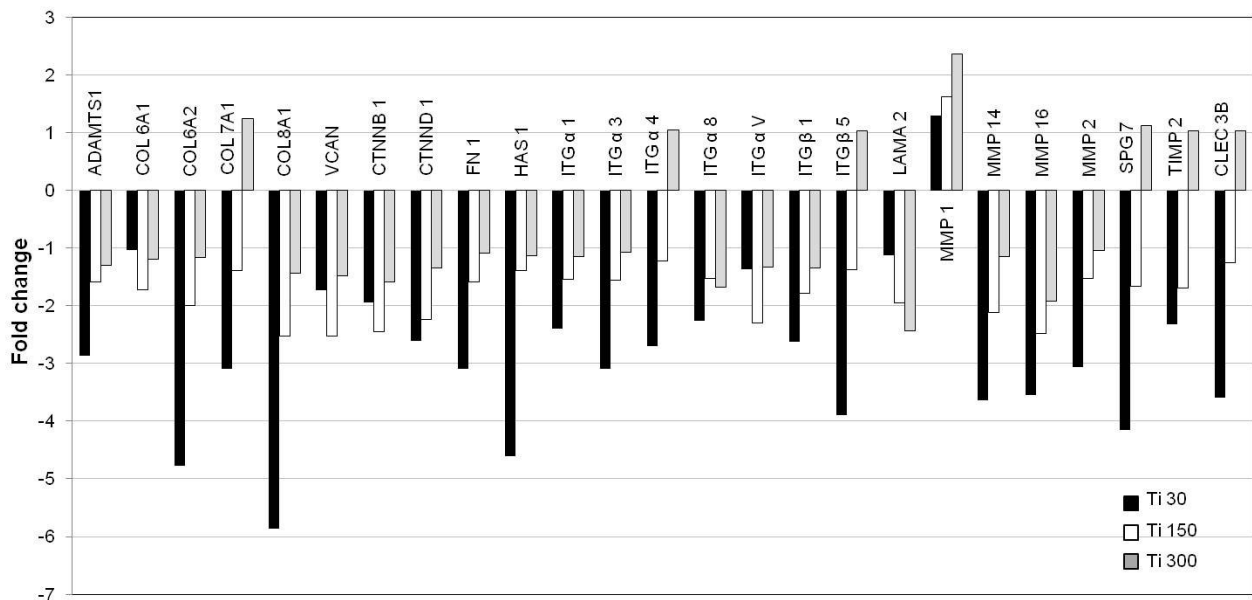


Fig. 4. Human extracellular matrix and adhesion molecule PCR array results for hMSCs cultured on plain control (Ti) and nanostructured surface (Ti30, Ti150 and Ti300) for 1 d. The result was expressed in fold change with Value 0 for Ti.

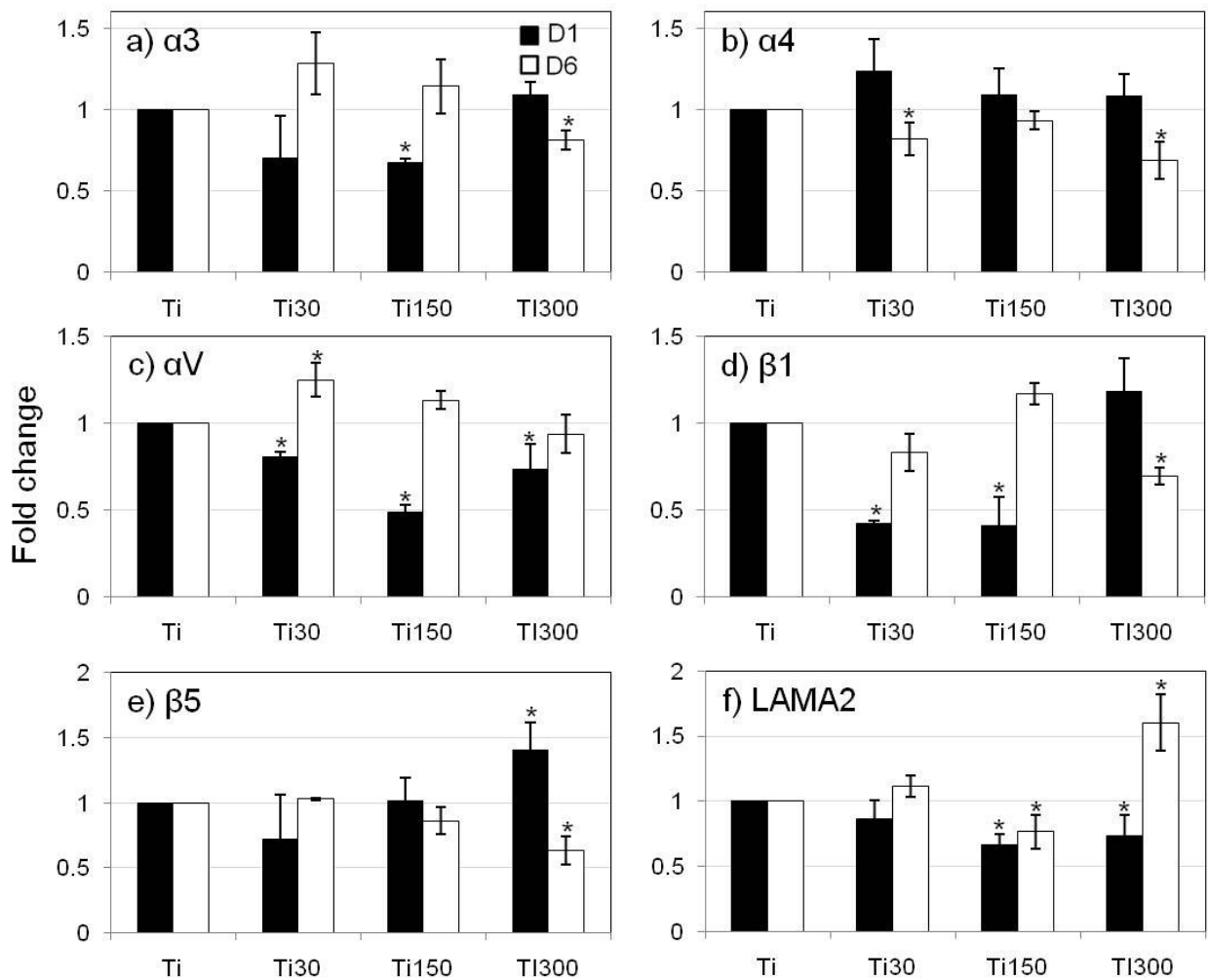


Fig. 5. Effects of nanostructured titanium surface on mRNA expression of selected adhesion genes in hMSCs cultured for 1 and 6 d on Ti substrate (Ti, Ti30, Ti150 and Ti300). RT-PCR of mRNA of (a) Integrin subunit α3; (b) Integrin subunit α4; (c) Integrin subunit αV; (d) Integrin subunit β1; (e) Integrin subunit β5 and (f) LAMA2 normalised by RPL19. * $p < 0.05$, Ti nano vs. Ti.

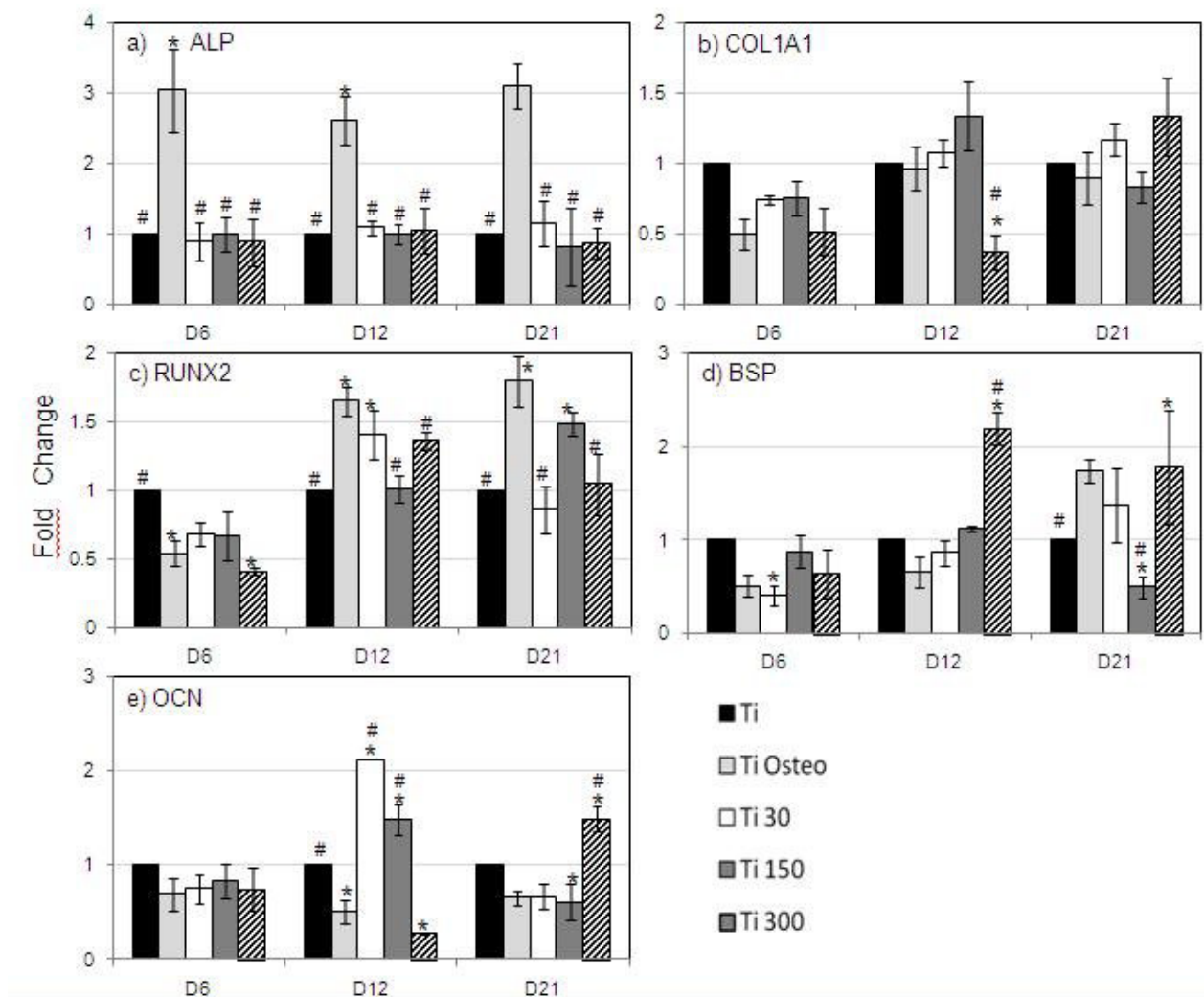


Fig. 6. Effects of nanostructured titanium surface on mRNA expression of osteogenic genes in hMSCs cultured for 1 and 6 d on Ti substrate without osteogenic factor (Ti, Ti30, Ti150 and Ti300) and with osteogenic factor (Ti osteo). RT-PCR of mRNA of (a) ALP; (b) COL1A1; (c) RUNX2; (d) BSP, and (e) OCN. * $p < 0.05$, Ti nano vs. Ti.

Integrin and extracellular matrix gene expression

Following the significant effect of nanotopography observed on hMSC morphology, adhesion and extracellular matrix, molecule RT² Profiler PCR arrays were used to decipher particular gene expression on Ti, Ti30, Ti150 and Ti300 surfaces (Fig. 4). The arrays profiled the expression of 84 genes important for cell-cell and cell-matrix interactions. Since the most prominent differences in cell morphology were observed after day 1, PCR arrays were conducted at this culture period. Planar Ti was used as the control surface and was set at null. The expression of 61 genes was unaffected with a range of variation two times lower than for cells on Ti30, Ti150 and Ti300 as compared to Ti, while 25 genes were over or under expressed on nanoporous titanium surfaces compared to plain surfaces (Fig. 4). In particular, 18 genes were more under expressed on Ti 30 than on the other surfaces, including 3 collagens (COL6A1, COL7A1, COL8A1), 6 integrins and 4 metalloproteases (MMP2, MMP14, MMP16 and SPG7 MMP). In contrast, on Ti150, only 3 genes (VCAN, CTNBNB1, ITG α V) were slightly underexpressed compared to the other surfaces. On

Ti300, 6 genes (COL7A1, ITG α 4, ITG β 5, SPG7, TIMP2 and CLEC3B) were over expressed as compared with Ti30 and Ti150 and MMP1 was expressed more than as much as on the Ti surface. The nanostructured surfaces influenced cell adhesion by modulating the expression of integrins and other extracellular matrix molecules. In order to confirm the PCR array results, quantitative polymerase chain reaction (qPCR) was used with primers for integrin subunits α 3, α 4, α V, β 1 and β 5 and laminin A2 (LAMA2). The RT-qPCR was performed after 1 and 6 d of culture (Fig. 5), as for cell morphology and focal point density. In agreement with the PCR array analysis, hMSC cultured on nanostructured surfaces were expressed differently depending on the surface. Slight differences in variation were observed for subunit α 3 (Fig. 5). Nevertheless, this subunit was less expressed after 1 d but more expressed after 6 d for Ti30 and Ti150 as compared to control. The expression of this gene was similar for Ti300 and the control after day 1 and slightly lower at day 6. No significant difference was observed for the expression of subunit α 4 after day 1 whereas it was lower at day 6 for Ti30 and Ti300. Subunit

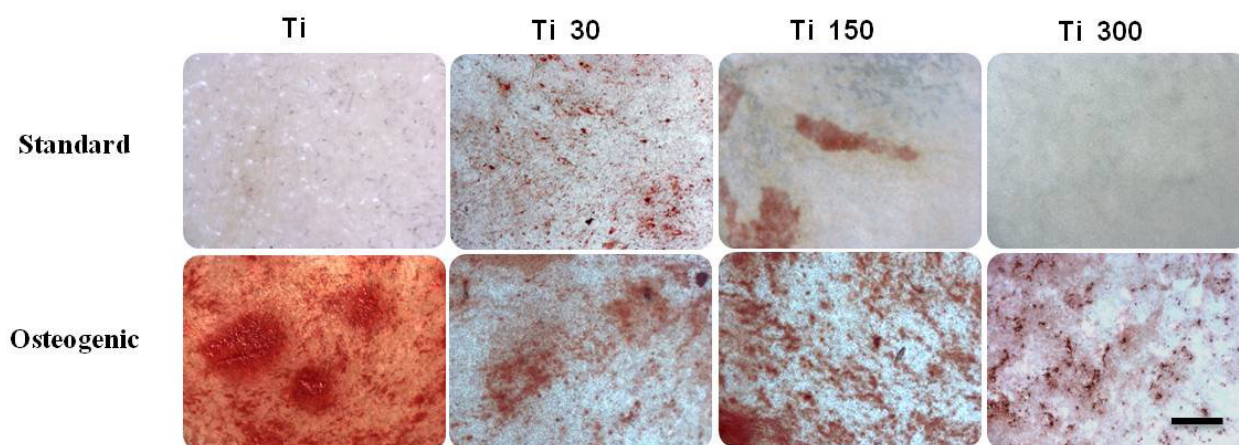


Fig. 7. Alizarin red staining in control and osteogenic media for hMSCs on control Ti and nanostructured Ti30, Ti150 and Ti300 substrates after 28 d of culture (scale bar: 1000 μ m).

α V was less expressed on nanostructured titanium surfaces at day 1, but appeared more expressed on Ti30 at day 6. Subunit β 1 exhibited the most striking variations with less expression for Ti30 and Ti150 at day 1, and inversely more expression for Ti150 at day 6 and Ti300 at day 1. No difference in subunit β 5 gene expression was observed on Ti30 or Ti150 at either time. For Ti300, it was firstly more and then less expressed. Laminin 2 expression was similar to the control for Ti0, lower for Ti150 at the two time points, but respectively less and more expressed on Ti300 after days 1 and 6.

Osteogenic differentiation on nanostructured Ti surfaces

Titanium nanostructure may also control hMSC differentiation. Osteogenic differentiation of hMSCs cultured on nanostructured Ti (Ti nano) was investigated using RT-qPCR after 6, 12 and 21 d of culture. Ti nano gene expression was compared to plain Ti in standard and osteogenic culture conditions. The RT-qPCR results are shown in Fig. 6 after normalisation with the negative Ti control.

Despite ALP induction in osteogenic conditions (Ti osteo), we did not observe any differences on Ti nano. However for genes up-regulated during osteoblastic differentiation, we observed differences between the surfaces at different times. No significant differences were observed on any Ti surfaces compared to the control at all time periods, except for the expression of COL1A1 which was even lower for Ti300 at day 12 than for the positive and negative control (Ti osteo and Ti). At day 12, RUNX2 was more expressed on Ti30 and Ti300 compared to Ti. In comparison to osteogenic conditions (Ti osteo), RUNX2 expression on Ti30 and Ti300 was similar at day 6 and 12. At day 21, however, RUNX2 expression on Ti150 was similar to the positive control (Ti osteo). For the BSP gene, early up-regulation was observed for Ti300 only compared to Ti osteo and other surfaces. Conversely, BSP on Ti 30 was equivalent to its expression on the positive control (Ti osteo) at all time periods. OCN expression did not change on days 6 and 12 in osteogenic conditions as compared to

the negative control. However, an up-regulation of OCN was induced by Ti30 and Ti150 as early as day 12 and for Ti300 at day 21. The general trend was that pore size induced up-regulation of genes involved in osteoblastic differentiation such as RUNX2, BSP and OCN. This regulation was similar or early compared to osteogenic condition.

In an attempt to test matrix mineralisation, alizarin red S staining was performed in standard and osteogenic culture conditions after 28 days (Fig. 7). Staining for mineralisation was negative for cells cultured in standard medium on Ti and Ti300, while positive staining was observed on Ti30 and Ti150 and seemed to be greater on Ti30. In osteogenic conditions, alizarin staining was positive for cells cultured on all substrates.

Discussion

It has recently been shown that nanometre-sized features control cell adhesion and osteogenic differentiation (Assoian *et al.*, 1997), although these results have not been confirmed on nanostructured titanium. Theoretically, an ideal titanium implant would encourage stem cells to differentiate into mature osteoblasts for direct bone apposition, rather than fibroblastic cells resulting in fibrous tissue encapsulation. It has been established that integrins are the links between cells and ECM and serve as signal transducers for regulating cell growth, differentiation and motility (Damsky and Werb, 1992; Clark *et al.*, 1995; Lafrenie and Yamada, 1996; Kumar, 1998; Wang *et al.*, 2006). In this study, nanostructured titanium with 30, 150 and 300 nm pores as well as plain Ti control served as substrates for culturing hMSCs. After 1 d, hMSCs exhibited differences in cell morphology as a function of surfaces. Cells had a predominantly typical spindle shape. On the Ti30 surface, hMSCs exhibited mainly a branched shape whereas the percentages of branched and spindle cells were comparable for Ti150. Focal point density was greater on Ti30 and Ti300. These surfaces seemed more suitable for cell adhesion. qPCR indicated that the nanostructure

slightly influenced integrin expression, which is prominent in cell adhesion. Mineralisation staining was negative for cells cultured in standard medium on Ti and Ti300 while positive staining was observed on Ti30 and Ti150 and seemed greater on Ti30. Overall, the Ti30 surface was the most potent nanostructure for osteogenic differentiation of hMSCs.

In this study, we were able to notice differences in gene expression depending on titanium pore size with PCR array for adhesion and extracellular molecules. These variations concerned integrin, collagen and metalloproteinase expression. hMSCs cultured on Ti150 and Ti300 seemed to behave similarly, whereas Ti30 was different. As integrins are receptor molecules for extracellular matrix molecules (*e.g.*, the β_1 family), serum components (α_v family) and immunoglobulin family adhesion molecules (β_2 family), these molecules are obviously critical in cell behaviour. Previous studies have identified that integrin β_1 is required for osteoblastic differentiation on microscale Ti substrates (Olivares-Navarrete *et al.*, 2008; Chuluyan *et al.*, 1995). β_1 integrin recognises that the VCAM-1 counter receptor presents on endothelial cells and ECM proteins such as fibronectin, collagen and vitronectin (Issekutz, 1995; Meerschaert and Furie 1995; Lai *et al.*, 2000). Moreover, TGF- β increases expression of the integrin β_5 gene in osteoblastic cell lines by mechanisms involving Sp1/Sp3 and Smad transcription factors (Hughes *et al.*, 1993). In our study, we observed slight but significant variations in α_3 , α_4 subunits and α_v expression, as well as sub-units β_1 and β_5 . For instance, α_3 and α_v subunits were less expressed on Ti30 and Ti150 at day 1 and then at day 6, no variation with the control was observed. Integrin expression after 1 and 6 d of culture seemed to be similar for 30 or 150 nm pore sizes. The correlation between integrin expression and hMSC differentiation in the context of their interactions with biomaterial surfaces has been poorly investigated. Most available studies concern differentiated cells. For instance, it has been found that osteoblasts at the bone surface express high levels of $\alpha_5\beta_1$, $\alpha_v\beta_3$ and $\alpha_v\beta_5$ (Hultenby *et al.*, 1993; Humphries *et al.*, 2006) while osteoblast adhesion to vitronectin is mediated specifically by $\alpha_v\beta_5$. $\alpha_5\beta_1$ integrin is a cell surface receptor for fibronectin that has been implicated in cell spreading, proliferation, differentiation, migration, and survival in different cell types (Moursi *et al.*, 1997; Gingras *et al.*, 2006; Hamidouche *et al.*, 2009). However, blocking $\alpha_5\beta_1$ integrin using antibodies did not affect the differentiation of osteoblasts cultured on rough Ti, suggesting that an alternate integrin partner may be involved (Moursi *et al.*, 1997; Gingras *et al.*, 2006; Hamidouche *et al.*, 2009).

Cell adhesion by means of integrins to a variety of extracellular matrix proteins, such as fibronectin, collagen and laminin, is a potent regulator of cell growth, differentiation, and gene expression. When integrins bind to ECM proteins, they physically link the ECM to the actin cytoskeleton (Damsky and Werb, 1992). Ligand binding on integrins initiates a number of metabolic changes including activation of serine/threonine and tyrosine kinases, increased Ca^{2+} influx, increased cytoplasmic alkalinisation, altered inositol lipid metabolism and changes in cell morphology (Wang *et al.*, 2006). In addition, adhesion-

dependent signalling pathways that regulate the actin cytoskeleton are also required for many of the functional responses elicited by integrin-mediated cell adhesion. The talin and actin-binding protein vinculin and focal adhesion tyrosine kinase (FAK) are incorporated next to the focal adhesion complex, strengthening the ECM-cytoskeleton contact across the integrin. The vinculin binding site exposed in the talin rod (Hvidt, 1991), incorporated with talin-bound actin (Arold *et al.*, 2002), activates vinculin. The vinculin tail domain also interacts with paxillin, which is involved in ECM-bound integrin recruitment (Hayashi *et al.*, 2002; Zaidel-Bar *et al.*, 2003). Recruitment of the actin-bonding homodimer α -actinin is a later event in the formation of focal adhesion (McBeath *et al.*, 2004). No difference in cell morphology was observed after a few hours but differences were clearly visible after 1 d of culture on the substrates. hMSCs had a predominantly typical spindle shape on Ti and Ti300. On the Ti30 surface, hMSCs exhibited mainly a branched shape whereas the percentages of branched and spindle cells were comparable for Ti150. These differences in cell morphology corroborated that cells on Ti30 exhibited a different compartment than on Ti, Ti150 and Ti300 as shown for gene expression. Overall, the Ti30 surface seemed to induce a branched morphology with more numerous focal points than in other nanostructures.

While differentiation may cause changes in cell shape, several studies have noted that cell morphology can also alter the differentiation of mesenchymal lineage (Lavenus *et al.*, 2010). It has been shown that round cells promote adipogenesis while cells with high spreading prefer an osteoblast fate. These studies demonstrated that mechanical cues embodied in cell shape, cytoskeletal tension and RhoA signalling are integral to the commitment of stem cell fate (Lavenus *et al.*, 2010). In our work, hMSCs spread considerably with a branched morphology on Ti30 at 1 d of culture while on the other substrate the shape was predominately spindle. This branched shape may increase the contractility of the cytoskeleton and lead to preferential osteoblastic differentiation. Similarly, it has been shown that the round shape induces low contractibility resulting in adipocyte differentiation of MSCs (Kilian *et al.*, 2010). The spindle morphology observed on the other substrates may be due to a non-differentiating state or fibroblastic lineage of MSCs. In our study, the Ti30 nanostructure induced branched morphology that may promote osteogenic differentiation.

In order to validate the hypothesis that nanostructure influenced cell differentiation, we studied osteogenic gene expression by RT-qPCR and mineralisation by red alizarin staining on the different substrates. A previous study considering hMSC differentiation and topography was carried out using nanometre roughness and hMSCs at 14 d (Dalby *et al.*, 2007b). In this study, the authors demonstrated that nanoscale disorders stimulated (2 fold) osteoblastic gene expression (OCN and ALP) in the absence of osteogenic factors. In agreement with this study, we showed that the nanopore caused slight but significant changes in osteoblastic gene expression in a size-dependent manner. We found that cells proliferated up to 6-12 d and started to produce early differentiation markers (OCN, OPN, BSP) in agreement with other studies (Stein and Lian,

1993). By day 28, mineralisation was clearly visible on Ti30 and Ti150 nanostructures without osteogenic factor. Additionally, the nanostructures seemed to promote the differentiation of hMSCs into osteoblastic cells.

Considering titanium implant surfaces, these nanostructures may direct osteogenic differentiation of stem cells for direct bone apposition. Cells arriving on implant surfaces express differently integrins that have an impact on cytoskeleton tension. Such changes in cytoskeleton tension will have a direct effect on cell morphology observed by actin staining. The changes in cells morphology caused by cytoskeletal tension have an indirect effect on mechanotransduction pathways, as demonstrated by changes in RhoA expression in MSCs' response to hardness material (Kilian *et al.*, 2010; Lavenus *et al.*, 2010; Chen *et al.*, 1997). It has also been speculated that changes in cytoskeletal tension in response to topography may modify interphase nucleus organisation and hence more directly influence cell gene expression profiles (Curtis *et al.*, 2007; Dalby *et al.*, 2007b). Although nanostructures have an effect on the osteogenic differentiation of stem cells, the results should be confirmed by *in vivo* experiments studying the bone tissue integration of implants.

Conclusion

In this study, we demonstrated the influence of nanopores on the behaviour of human mesenchymal stem cells. In particular, the expression of integrins, cell morphology and osteoblastic differentiation was affected by the nanostructured titanium surface. The expression of integrins was slightly but significantly modulated by nanopore size on titanium. hMSCs exhibited as early as day 1 a more branched cell morphology on the Ti30 surface than on other surfaces. Moreover, the most potent nanostructure for osteogenic differentiation consisted of Ti30 and Ti150 while the Ti300 had a limited effect. Nanopores of 30 nm may promote early osteoblastic differentiation and, consequently, rapid osseointegration of titanium implants.

Acknowledgements

The authors would like to thank R. Bareille and J. Amédée for their technical assistance with cell immunostaining. Paul Pilet and the microscopy centre of U791 are acknowledged for help with image analysis. The European Council has financially supported part of this study through the European project Reborne #241879 in the 7th Framework program. Inserm, SFBTM and the French Ministry of Research are acknowledged for supporting the PhD thesis of S. Lavenus. The authors are grateful to Kirsty Snaith of Medicis Traduction for grammar and spelling corrections of the manuscript.

References

Arold ST, Hoellerer MK, Noble MEM (2002) The structural basis of localization and signaling by the focal adhesion targeting domain. *Structure* **10**: 319-327.

Assoian RK, Zhu X (1997) Cell anchorage and the cytoskeleton as partners in growth factor dependent cell cycle progression. *Curr Opin Cell Biol* **9**: 93-98.

Cai K, Bossert J, Jandt, KD (2006) Does the nanometre scale topography of titanium influence protein adsorption and cell proliferation? *Colloids Surf B: Biointerfaces* **49**: 136-144.

Caplan AI (2009) Why are MSCs therapeutic? New data: new insight. *J Pathol* **217**: 318-324.

Caplan AI, Dennis JE (2006) Mesenchymal stem cells as trophic mediators. *J Cell Biochem* **98**: 1076-1084.

Chen CS, Mrksich M, Huang S, Whitesides GM, Ingber DE (1997) Geometric control of cell life and death. *Science* **276**: 1425-1428.

Chuluyan HE, Schall TJ, Yoshimura T, Issekutz AC (1995) IL-1 activation of endothelium supports VLA-4 (CD49d/CD29)-mediated monocyte transendothelial migration to C5a, MIP-1 alpha, RANTES, and PAF but inhibits migration to MCP-1: a regulatory role for endothelium-derived MCP-1. *J Leukoc Biol* **58**: 71-79.

Clark EA, Brugge JS (1995) Integrins and signal transduction pathways: the road taken. *Science* **268**: 233-239.

Curtis AS, Varde M (1964) control of cell behavior: topological factors. *J Natl Cancer Inst* **33**: 15-26.

Curtis A, Sokolikova-Csaderova L, Aitchison G (2007) Measuring cell forces by a photoelastic method. *Biophys J* **92**: 2255-2261.

Curtis ASG, Casey B, Gallagher JO, Pasqui D, Wood MA, Wilkinson CDW (2001) Substratum nanotopography and the adhesion of biological cells. Are symmetry or regularity of nanotopography important? *Biophys Chem* **94**: 275-283.

Dalby MJ, McCloy D, Robertson M, Wilkinson CDW, Oreffo ROC (2006a) Osteoprogenitor response to defined topographies with nanoscale depths. *Biomaterials* **27**: 1306-1315.

Dalby MJ, McCloy D, Robertson M, Agheli H, Sutherland D, Affrossman S, Oreffo ROC (2006b) Osteoprogenitor response to semi-ordered and random nanotopographies. *Biomaterials* **27**: 2980-2987.

Dalby MJ, Gadegaard N, Curtis ASG, Oreffo ROC (2007a) Nanotopographical control of human osteoprogenitor differentiation. *Curr Stem Cell Res Ther* **2**: 129-138.

Dalby MJ, Gadegaard N, Herzyk P, Sutherland D, Agheli H, Wilkinson CD, Curtis AS (2007b) Nanomechanotransduction and Interphase Nuclear Organization influence on genomic control. *J Cell Biochem* **102**: 1234-1244.

Damsky CH, Werb Z. (1992) Signal transduction by integrin receptors for extracellular matrix: cooperative processing of extracellular information. *Curr Opin Cell Biol* **4**: 772-781.

Davies JE (2003) Understanding peri-implant endosseous healing. *J Dent Educ* **67**: 932-949.

Engler AJ, Sen S, Sweeney HL, Discher DE (2006) Matrix elasticity directs stem cell lineage specification. *Cell* **126**: 677-689.

Gingras AR, Vogel KP, Steinhoff HJ, Ziegler WH, Patel B, Emsley J, Critchley DR, Roberts GC, Barsukov

- IL (2006) Structural and dynamic characterization of a vinculin binding site in the talin rod. *Biochemistry* **45**: 1805-1817.
- Hamidouche Z, Fromigue O, Ringe J, Haupl T, Vaudin P, Pages JC, Srouji S, Livne E, Marie PJ (2009) Priming integrin $\alpha 5$ promotes human mesenchymal stromal cell osteoblast differentiation and osteogenesis. *Proc Natl Acad Sci USA* **106**: 18587-18591.
- Hayashi I, Vuori K, Liddington RC (2002) The focal adhesion targeting (FAT) region of focal adhesion kinase is a four-helix bundle that binds paxillin. *Nat Struct. Biol* **9**: 101-106.
- Hughes DE, Salter DM, Dedhar S, Simpson R (1993) Integrin expression in human bone. *J. Bone Miner Res* **8**: 527-533.
- Hultenby K, Reinholt FP, Heinegård D (1993) Distribution of integrin subunits on rat metaphyseal osteoclasts and osteoblasts. *Eur J Cell Biol* **62**: 86-93.
- Humphries JD, Byron A, Humphries MJ. (2006) Integrin ligands at a glance. *J Cell Sci* **119**: 3901-3903.
- Hvidt S. (1991) Insulin association in neutral solutions studied by light scattering. *Biophys Chem* **39**: 205-213.
- Issekutz TB (1995) *In vivo* blood monocyte migration to acute inflammatory reactions, IL-1 α , TNF- α , IFN- γ , and C5a utilizes LFA-1, Mac-1, and VLA-4. The relative importance of each integrin. *J Immunol* **154**: 6533-6540.
- Kassem, M. (2006) Stem cells. potential therapy for age-related diseases. *Ann NY Acad Sci* **1067**: 436-442.
- Kilian KA, Bugarija B, Lahn BT, Mrksich M (2010) Geometric cues for directing the differentiation of mesenchymal stem cells. *Proc Natl Acad Sci USA* **107**: 4872-4877.
- Kumar CC (1998) Signaling by integrin receptors. *Oncogene* **17**: 1365-1373.
- Lafrenie RM, Yamada KM (1996) Integrin-dependent signal transduction. *J Cell Biochem* **61**: 543-553.
- Lai CF, Feng X, Nishimura R, Teitelbaum SL, Avioli LV, Ross FP, Cheng SL (2000) Transforming growth factor-beta up-regulates the $\beta 5$ integrin subunit expression via Sp1 and Smad signaling. *J Biol Chem* **275**: 36400-36406.
- Lavenus S, Ricquier JC, Louarn G, Layrolle P (2010) Cell interaction with nanopatterned surface of implants. *Nanomedicine (Lond)* **5**: 937-947.
- Lavenus S, Pilet P, Guicheux J, Weiss P, Louarn G, Layrolle P (2011) Behaviour of mesenchymal stem cells on smooth surfaces. *Acta Biomater* **7**: 1525-1534.
- Le Guéhennec L, Soueidan A, Layrolle P, Amouriq Y (2007) Surface treatments of titanium dental implants for rapid osseointegration. *Dent Mater* **23**: 844-854.
- Le Guehennec L, Lopez-Heredia MA, Enkel B, Weiss P, Amouriq Y, Layrolle P (2008a) Osteoblastic cell behaviour on different titanium implant surfaces. *Acta Biomater* **4**: 535-543.
- Le Guehennec L, Martin F, Lopez-Heredia MA, Louarn G, Amouriq Y, Cousty J, Layrolle P (2008b) Osteoblastic cell behavior on nanostructured metal implants. *Nanomedicine (Lond)* **3**: 61-71.
- Marco F, Milena F, Gianluca G, Vittoria O (2005) Peri-implant osteogenesis in health and osteoporosis. *Micron* **36**: 630-644.
- Marinucci L, Balloni S, Becchetti E, Bistoni G, Calvi EM, Lumare E, Ederli F, Locci P (2010) Effects of Hydroxyapatite and Biostite on Osteogenic Induction of hMSC. *Ann Biomed Eng* **38**: 640-648.
- McBeath R, Pirone DM, Nelson CM, Bhadriraju K, Chen CS (2004) Cell shape, cytoskeletal tension, and RhoA regulate stem cell lineage commitment. *Dev Cell* **6**: 483-495.
- Meerschaert J, Furie MB (1995) The adhesion molecules used by monocytes for migration across endothelium include CD11a/CD18, CD11b/CD18, and VLA-4 on monocytes and ICAM-1, VCAM-1, and other ligands on endothelium. *J Immunol* **154**: 4099-4112.
- Morganstein, DL, Wu P, Mane MR, Fisk NM, White R, Parker MG (2010) Human fetal mesenchymal stem cells differentiate into brown and white adipocytes: a role for ER α in human UCP1 expression. *Cell Res* **20**: 434-444.
- Moursi AM, Globus RK, Damsky CH (1997) Interactions between integrin receptors and fibronectin are required for calvarial osteoblast differentiation *in vitro*. *J Cell Sci* **110**: 2187-2196.
- Olivares-Navarrete R, Raz P, Zhao G, Chen J, Wieland M, Cochran DL, Chaudhri RA, Ornoy A, Boyan BD, Schwartz Z (2008) Integrin $\alpha 2\beta 1$ plays a critical role in osteoblast response to micron-scale surface structure and surface energy of titanium substrates. *Proc Natl Acad Sci USA* **105**: 15767-15772.
- Olivares-Navarrete R, Hyzy SL, Hutton DL, Erdman CP, Wieland M, Boyana BD (2010) Direct and indirect effects of microstructured titanium substrates on the induction of mesenchymal stem cell differentiation towards the osteoblast lineage. *Biomaterials* **31**: 2728-2735.
- Protivinský J, Appleford M, Strnad J, Helebrant A, Ong JL (2007) Effect of chemically modified titanium surfaces on protein adsorption and osteoblast precursor cell behavior. *Int J Oral Maxillofac Implants* **22**: 542-550.
- Stein GS, Lian JB (1993) Molecular mechanisms mediating proliferation/ differentiation interrelationships during progressive development of the osteoblast phenotype. *Endocr Rev* **14**: 424-442.
- Stevens MM, George JH (2005) Exploring and engineering the cell surface interface. *Science* **310**: 1135-1138.
- Wang L, Zhao G, Olivares-Navarrete R, Bell BF, Wieland M, Cochran DL, Schwartz Z, Boyan BD (2006) Integrin $\beta 1$ silencing in osteoblasts alters substrate-dependent responses to 1,25-dihydroxy vitamin D₃. *Biomaterials* **27**: 3716-3725.
- Watson PA (1991) Function follows form: generation of intracellular signals by cell deformation. *FASEB J* **5**: 2013-2019.
- Yang Y, Tian J, Deng L, Ong JL (2002) Morphological behavior of osteoblast-like cells on surface-modified titanium *in vitro*. *Biomaterials* **23**: 1383-1389.
- Zaidel-Bar R, Ballestrin C, Kam Z, Geiger B (2003) Early molecular events in the assembly of matrix adhesions at the leading edge of migrating cells. *J Cell Sci* **116**: 4605-4613.
- Zannettino A, Paton S, Arthur A, Khor F, Itescu S, Gimble J, Gronthos S (2008), Multipotential human

adipose-derived stromal stem cells exhibit a perivascular phenotype *in vitro* and *in vivo*. *J Cell Physiol* **214**: 413-421.

Zhao G, Raines AL, Wieland M, Schwartz Z, Boyan BD (2007) Requirement for both micron- and submicron scale structure for synergistic responses of osteoblasts to substrate surface energy and topography. *Biomaterials* **28**: 2821-2829.

Discussion with Reviewers

Reviewer II: The surface characterisation is deceiving, because the authors do not pay the required attention to the chemical and topographic characterisation. In fact, it looks that the Ti evaporation does not respect at all the

polycarbonate membrane topography. The Ti30 images present less pores, but not smaller than those of Ti150. Furthermore, the porosity and oxidation of the Ti layers could be very much related. This could have an influence on the cell adhesion results! Please comment.

Authors: We do not agree with the referee on this point. We have used X-ray photoelectron spectroscopy and scanning electron microscopy (SEM) to characterise both the chemistry and topography of the samples (see Fig. 1). These analyses clearly demonstrated that a titanium layer that was covered by a thin titania layer after exposure to air was formed. Titania covers all implants made of titanium being used in dentistry or orthopaedics. Furthermore, the scale of photographs in Fig. 1 is different and the pores of Ti30 and Ti150 have different diameters.